Evaluation of Power Receiving Signal of 5G Small Cells for Outdoor/Indoor Environment at Millimeterwave Bands

Nagham Hamid

University of Information Technology and Communications
College of Business Informatics, Baghdad, Iraq
nagham.finjan@uoitc.edu.iq

Abstract ─ This paper presents a simulation study of the outdoor and indoor propagation losses utilizing 5G small cells at suggested millimeter-wave frequencies of 26 GHz, 28 GHz, and 38 GHz. The environment of this study is conducted with penetration loss of new and old building characteristics. The simulation is performed with help of 3D ray tracing model NVIDIA OptiX engine and MATLAB. The targeted frequencies are 26 GHz, 28 GHz, and 38 GHz that specified by International Telecommunication Union ITU-R organization. The simulation routes are investigated in term of signal strength at multiple receiving points. The strength angular spectrum are represented for fixed points and the power receiving delay is presented by their attributes. The simulated responses showed an efficient and sufficient outdoor and indoor service might be provisioned at 26 GHz and 28 GHz. The received signals at 28 GHz and 38 GHz are found around 4.5 dB and 11 dB with comparison with signal received level at 26 GHz. However, at 38 GHz the indoor signal strength and power receiving delays demonstrate a weak signal reception which offers a poor solution to indoor user by outside fixed base station.

Index Terms ─ 5G small cell, millimeter-wave, NVIDIA OptiX, penetration loss, propagation loss.

I. INTRODUCTION

Currently, the fifth generation (5G) mobile networks are shifted toward standardization. The 5G mobile technology is delivered as a part of general 5G requirements with 3GPP Release [1]. Moreover, 5G technology is investigated in both academic and industry fields [2]. The recent researches cover 5G technology utilizing substantial multiple input multiple-output (MIMO) techniques, radio and air-interface access system (RAN), and beamforming networks [3-5]. The 5G technology requirements are higher capacity, huge bandwidth, high gain, directive antennas, compact antenna size, high receiving sensitivity, and high efficiency [6]. As such the frequency bands under 4 GHz suffer from overloaded users due to the latest mobile network technologies. Therefore, the main aim of 5G technology is to provide huge bandwidth by using millimeter-wave frequencies ranging from 3 GHz to 300 GHz.

In addition, it is estimated that the mobile information traffic will be rapidly increased by the mid of 2022 as a result of implementing smart technology in the internet of things (IoTs) technology [7]. Thus, to provide a wide bandwidth and coverage, the cellular network is shifted toward millimeter-wave frequencies such as 26 GHz, 28 GHz, 38 GHz, and 60 GHz [8]. In these proposed frequencies, the development of small or ultra-small cells is further investigated. Several issues and challenges are raised when it comes to small cells including the importance of handover (HO) factor. One of the challenges is related to the high path loss of millimeter-wave technology. As utilizing millimeter-wave wavelength increases the path loss [9]. As example, if an isotropic antenna is used as transmitter and receiver edge, the receive signal is around 20 dB at 3 GHz and 30 GHz respectively. This is due to the aperture antenna size based on the antenna wavelength. Hence, the aperture antenna size at 3 GHz will be repaired to utilize being an antenna array of 30 GHz. Hence, the difference between the power transmitted and received will be zero [10]. Therefore, several studies are done to increase the directivity of the antenna and reduces the path loss effects [11-13]. The other challenge is the multipath propagation at millimeter-wave frequencies. The traditional propagation prediction designs lack the attentiveness information about channel circumstances such as the model environment. The 3D ray tracing models providing these information such as reflections from walls, diffraction from building edges, scattering from small obstacles, and penetration models (concrete, glass) [14, 15]. Hence, the 3D ray tracing model is a potential tool to locate a multipath propagation characteristics between the transmitter and the receiver.

Therefore, this work aims to analyze and investigate the multipath propagation attributes of small cell for 5G cellular networks. The tested cell is chosen from Al Yarmouk Teaching Hospital locating in Baghdad, Iraq. The targeted frequencies are 26 GHz, 28 GHz, and 38 GHz frequency bands. A 3D ray tracing engine named

Submitted On: August 23, 2020
Accepted On: January 18, 2021

https://doi.org/10.47037/2020.ACES.J.360210

"NVIDIA OptiX" is used for simulation process with help of 3D ray tracing for indoor radio propagation code provided by MATLAB [16]. This paper also presents a genuine yard with old and new building model from Baghdad, Iraq.

II. PROFILE MODELLING OF THE STUDY

The simulations are done in this research follows the steps configuration provided in [17]. The obtained results of the 5G system configuration in [17] are found in [18]. The mentioned configuration are limited to 15 GHz. However, this analysis covers 26 GHz, 28 GHz along with 38 GHz. The realized 5G configuration have four contiguous carriers (CCs) providing a 100 MHz bandwidth and a carrier aggregation (CA) with bandwidth of 400 MHz. A 30.5 dBm power transmitted per CC is used, which leads to a total power of 35.3 dB of CC configuration. A transmitted directional antenna placed on the roof of the suggested building at 8 m height and tilted with 4° as shown in Fig. 1. The half power beamwidth in both direction (H and V directions) is selected to be 90° and 10.5° respectively. The chosen antenna gain for this study is configured to be 14.5 dBi.

Fig. 1. The google map of the targeted buildings.

Simulations are carried out by using a NVIDIA OptiX 3D ray tracing tool for outdoor and MATLAB code for indoor. Different than other quasi-3D ray tracing models, NVIDIA OptiX works full three dimensional ray tracing. In case of reflection paths, the reflection is provided by the reflection coefficients. The diffracted paths with its parameters are provided in this study. In such way, the scattering power is distributed in a broad range of directions. Moreover, the effect of scattering becomes substantial in higher frequencies. Thus, a concentric circle approach given at [19-21] is used to produce scattering areas on the walls of structures.

The NVIDIA OptiX 3D ray tracing simulation tool offers a various qualities of propagation of multipath plus supplies the outcomes resulting as form of standard crucial functionality signals (KPIs) including signal receiving strength. Similarly, the signal-to-noise-and-interference ratio (SINR) is also tested. The main aim is studying the signal receiving and propagation inside a small cell structure. Therefore a location of Al Yarmouk Teaching Hospital locating in Baghdad, Iraq is used for simulation. The Google chart perspective of the goal area is shown in Fig. 1. A representing model of two-dimensional graph of the proposed buildings area is represented in Fig. 2.

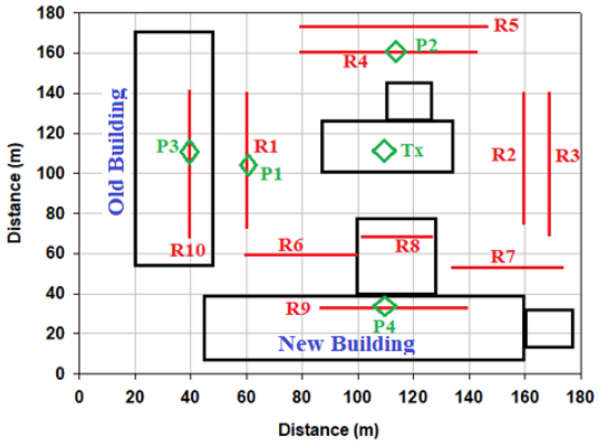

Fig. 2. A 2D representation of the Buildings.

In this proposed scenario, it has been assumed that the user carried a mobile with a height of 1.87 m for indoor and outdoor simulations. In the same time, it has been assumed that the user is always keep moving around and inside the tested area and buildings. A 7 outdoor routes denoted as (R1-R7) and 3 indoor routes denoted as (R8-R10) are marked with red lines as seen in Fig. 2. Four power receiving fixed points are placed in different locations as two outdoors (P1-P2) and two indoor points (P3-P4) for power angular spectrum (PAS) evaluation. At the front of the transmitter antenna, two paths are directly placed and two paths are placed at the back of the antenna transmission spot. The actual the transmitter (TX) antenna is marked with a green dot. Hence, the transmitter antenna is facing west direction towards first building. It's assumed that a directive antenna holding a receiver edge at a level of 1.87 m is turned by 360° within the azimuth with a step tilt of 4°. The parameters configuration of the simulation process are summarized in Table 1. Beside the path loss of LOS, the penetration loss comes from signal penetrated from the outdoor to the indoor environment. Building Penetration Loss (BPL) generally referred to the

penetration loss comes from the outdoor to the indoor environment. The BPL can be defined as a function of frequency. Moreover, the general building are consists of concrete and standard glass walls, while the new building are commonly equipped with newly Infrared Reflective (IRR) glass windows. Therefore, The BPL is depending on the material characteristics used in the concrete and glass walls. Several studies are conducted to investigate the BPL with different types of materials [19-21]. The authors successfully modelled a standard equations for BPL in outdoor and indoor environment. The concrete walls BPL and glass walls frequency dependent can be found by [22-26],

$$L_{concrete} = 4 \times Frequency_{GHz} + 5 \text{ dB}, \quad (1)$$

$$L_{singleglass} = 0.1 \times Frequency_{GHz} + 1 \text{ dB}, \quad (2)$$

$$L_{doubleglass} = 0.2 \times Frequency_{GHz} + 2 \text{ dB}, \quad (3)$$

$$L_{IRR} = 0.3 \times Frequency_{GHz} + 3 \text{ dB}. \quad (4)$$

Table 1: Configuration parameters for the simulation process

Parameters	Value
Frequency	26, 28, 38 GHz
Single carrier component (CC) bandwidth	100 MHz
Transmission power per CC	30.5 dBm
Total transmission power	35.3 dBm
System bandwidth (4 CCs)	400 MHz
Transmitter height	8
Antenna down tilt	4°
Diffractions	1
Reflections	3

Rx distance with respect to Tx (m)									
R1	R2	R3	R4	R5	R6	R7	R8	R9	R10
50	50	60	50	60	50	60	40	70	70

As the building is composed of concrete and glass walls, the BPL total loss for old and new building can be calculated as [20]. Therefore, Fig. 3 shows the BPL total loss of different new and old building and at the targeted frequencies (26 GHz, 28 GHz, and 38 GHz):

$$L_{oldbuilding} = -10 \log_{10}\left[0.3 \times 10^{\frac{-L_{doubleglass}}{10}} + 0.7 \times 10^{\frac{-L_{concrete}}{10}}\right], \quad (5)$$

$$L_{newbuilding} = -10 \log_{10}\left[0.7 \times 10^{\frac{-L_{IRR}}{10}} + 0.3 \times 10^{\frac{-L_{concrete}}{10}}\right]. \quad (6)$$

As indoor environment consists of penetration loss comes from different type of glass such as single, double, and IRR glass walls, Fig. 4 shows the penetration loss in the indoor environment at desired millimeter-wave frequencies.

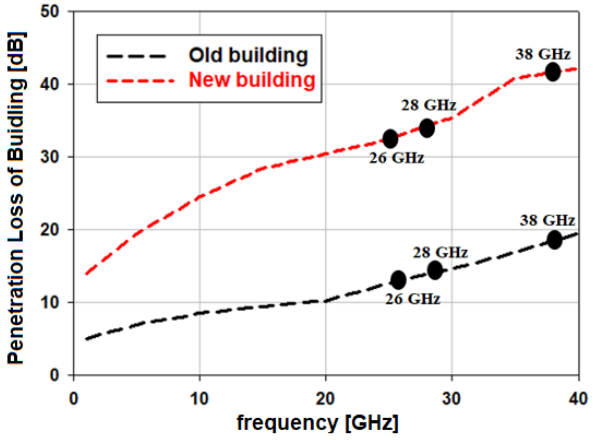

Fig. 3. The BPL of new and old building at desired frequencies.

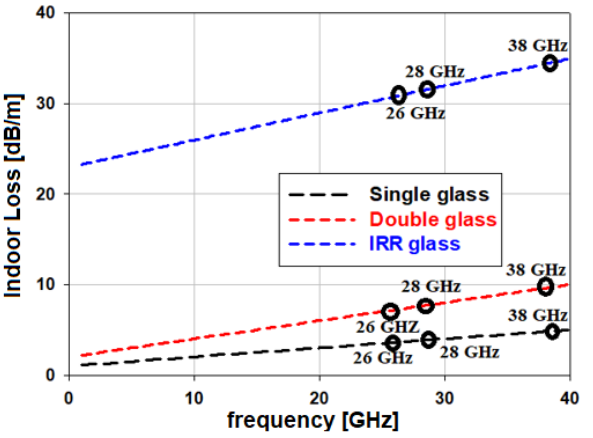

Fig. 4. Indoor loss for different type of glass at desired frequencies.

III. RESULTS AND DISCUSSIONS

Figures 5 (a), Fig. 5 (b), and Fig. 5 (c) display the received signal power in dBm for 7 outside routes and 3 indoor simulation routes at 26 GHz, 28 GHz, and 38 GHz respectively. It can be noticed that both R1 and R10 are in the main lobe of the transmitter antenna, while R2 and R3 are in the rear of the antenna. However, maximum signal amounts are achieved from simulation road at R1 with -42.54 dBm, whereas R2 is behind with the transmitter antenna and that's because of the low value of down tilt. The receive signal level of all paths at 26GHz, 28 GHz and 38 GHz are provided in Table 2. It is clearly seen that the signal level received at R1 route varies with the increasing of the frequency. The variance between 26 GHz and 28 GHz signal level at R1 is around 7.4 dBm, and 10 dBm between 28 GHz and 38 GHz. Most of the outdoor routes (R1-R7) have a signal receiving power ranging from -42.54 dBm to -80.27 dBm at different frequencies. Hence, the LOS path loss play a

key role when the frequency is increased. However, at 26 GHz and 28 GHz, the receiving power level is giving a promising solution utilizing the proposed 5G bands.

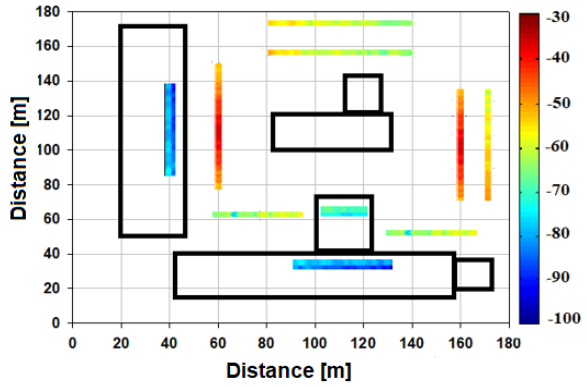

(a)

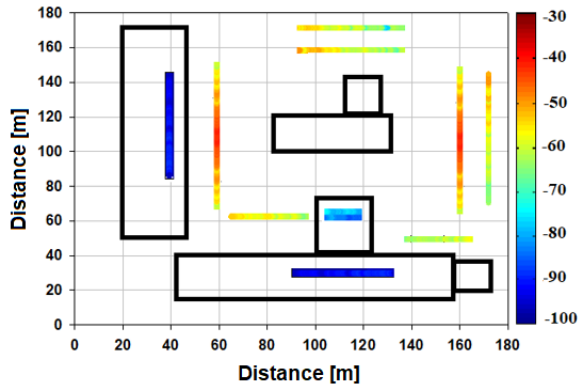

(b)

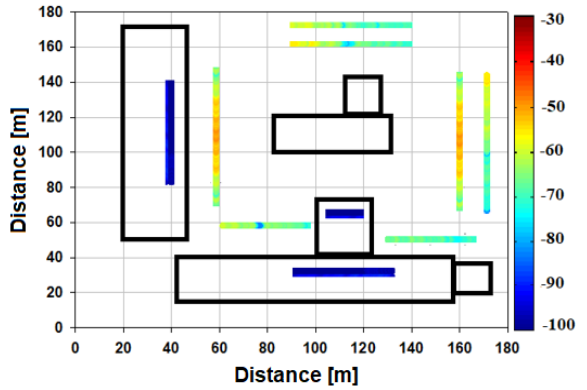

(c)

Fig. 5. The received signal map: (a) 26 GHz, (b) 28 GHz, and (c) 38 GHz.

In the indoor environment, the receiving power level is rapidly decreased. For instance, at 28 GHz and 38 GHz the signal level varies from -83.65 dBm to -125.02 dBm at (R8-R10) simulation routes. For example, the variance signal level between 26 GHz and 28 GHz at R9 route is around 10.7 dBm compared to the variance of 17 dBm between 28 GHz and 38 GHz. As mentioned earlier, the BPL in the building effects significantly when frequency is increased. Another effect of the BPL can be seen between R8 and R9 routes at 28 GHz. The variance between the two signal levels is around 16 dBm, while at 38 GHz is around 20 dB. That is caused by the losses come from the concrete and glass material beside the path loss of the LOS.

Table 2: Signal strength level at receiving points

Routes/ Frequency	**26 GHz**	**28 GHz**	**38 GHz**
R1	-42.54	-49.87	-59.66
R2	-45.36	-50.47	-60.24
R3	-56.21	-59.41	-70.87
R4	-59.47	-60.24	-72.57
R5	-62.35	-64.78	-73.87
R6	-66.89	-67.05	-79.87
R7	-70.25	-77.36	-80.27
R8	-82.47	-83.65	-96.87
R9	-88.98	-99.68	-125.05
R10	-92.45	-100.67	-110.2
Mean	-66.67	-70.31	-82.94
Standard deviations	16.25	18.02	20.29

Figure 6 shows the energy delay profile of P1-P4 at all desired frequencies. Both static areas are situated rather near one another therefore a nearly comparable PDP is obtained for equally areas. The multipath richness of environment is shown by a lot of multipath components. A comparable PDP is obtained for 28 GHz and 38 GHz. The mean delay for P1, P2, P3, and P4 are shown in Table 3. As can been noticed, the mean delays of P3 and P4 have similar values. This could be explained by the same distance of 70 m away from Tx at 38 GHz. The locations (R9 and R10) have similar multipath components as the height of the new building (R9) is same as the old building (R10). In such case, the height of location (R8) is lower with respect to the LOS and R9 height. A comparison is done in Table 4 between this work and other related works.

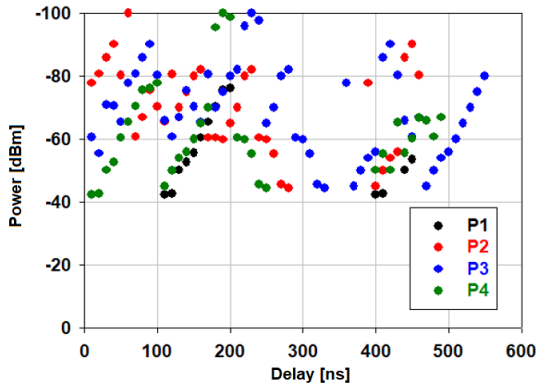

(a)

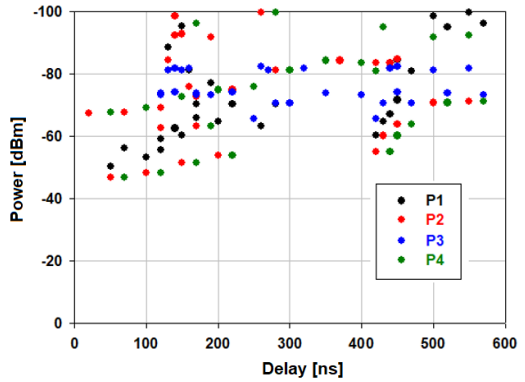

(b)

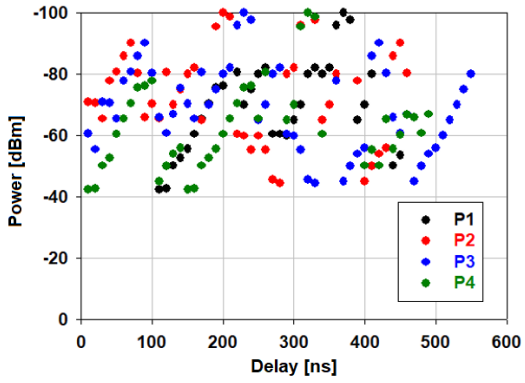

(c)

Fig. 6. Delay profile: (a) 26 GHz, (b) 28 GHz, and (c) 38 GHz.

Table 3: The mean delay (ns)

Power Received	26 GHz	28 GHz	38 GHz
P1	120	115	110
P2	124	119	115
P3	140	137	130
P4	150	140	130

Table 4: Comparison with other related works

Parameters	[24]	[26]	This work
Frequency (GHz)	15, 28, 60	0.8, 38	26, 28, 38
Max. received power (dBm)	-58	-45	-42.54
Min. received power (dBm)	-127	-80	-125.05
Mean delay (ns)	150	135	120
Outdoor routes	7	5	7
Indoor routes	4	2	3
Best scenario	15	0.8	26 GHz, 28 GHz
Location	Japan	Japan	Iraq
3D ray tracing model	SAGA	SAGA	NVIDIA OptiX

V. CONCLUSION

This paper presented an investigation for multipath propagation loss and model characteristics of power receiving levels for indoor and outdoor 5G small cell environment. The 5G small cell is conducted from genuine yard model from Baghdad, Iraq. The LOS and BPL are analysed with different receiving power points at targeted frequency of 26 GHz, 28 GHz, and 38GHz. The model consisted of seven outdoor routes and three indoor routes with one old building route and two new building routes. The maximum receiving power signal at LOS is around -42.54 dB at location R1 for 26 GHz, which is a LOS outdoor route while the minimum receiving power signal is around -80. 27 dBm at location R7 for 38 GHz. In the case of the indoor routes a poor receiving power signal achieved at routes R8-R10 with ranging of -82 dBm to -125 dB. This indicates that for outdoor 5G services it is a promising result for 26 GHz and 28 GHz bands. However, for services provided to indoor services, the receiving power signal suffers from BPL and diffraction losses. In such case, a directive and high gain antennas can be proposed as a solution for indoor services.

REFERENCES

[1] X. Wang, L. Kong, F. Kong, F. Qiu, M. Xia, S. Arnon, and G, Chen, "Millimeter wave communication: A comprehensive survey," *in IEEE Communications Surveys & Tutorials*, vol. 20, no. 3, pp. 1616-1653, 2018.

[2] J. Hirokawa, "Millimeter-wave antenna technologies for 5G mobile communication systems," *2016 IEEE International Workshop on Electromagnetics: Applications and Student Innovation Competition (iWEM)*, Nanjing, pp. 1-3, 2016.

[3] W. Hong, K.-H. Baek, Y. Lee, Y. Kim, and S.-T. Ko, "Study and prototyping of practically large-scale mmWave antenna systems for 5G cellular devices," *IEEE Commun. Mag.*, vol. 52, no. 9, pp. 63-69, 2014.

[4] J. Kim, M. Sung, S. Cho, Y. Won, B. Lim, S. Pyun, J. K. Lee, and J. Lee, 'MIMO-supporting radio-over-fiber system and its application in mmWave-based indoor 5G mobile network," *in Journal of Lightwave Technology*, vol. 38, no. 1, pp. 101-111, 2020.

[5] S. Buzzi, C. D'Andrea, A. Zappone, and C. D'Elia, "User-centric 5G cellular networks: Resource allocation and comparison with the cell-free massive MIMO approach," *in IEEE Transactions on Wireless Communications*, vol. 19, no. 2, pp. 1250-1264, 2020.

[6] N. Ojaroudiparchin, M. Shen, S. Zhang, and G. F. Pedersen, "A switchable 3-D-coverage-phased array antenna package for 5G mobile terminals," *in IEEE Antennas and Wireless Propagation Letters*,

vol. 15, pp. 1747-1750, 2016.

[7] D. Moongilan, "5G internet of things (IOT) near and far-fields and regulatory compliance intricacies," *2019 IEEE 5th World Forum on Internet of Things (WF-IoT)*, Limerick, Ireland, pp. 894-898, 2019.

[8] R. Q. Shaddad, F. Al-Kmali, M. Noman, N. Ahmed, E. Marish, A. Al-Duais, A. Al-Yafrsi, and F. Alsabri, "Planning of 5G millimeterwave wireless access network for dense urban area," *2019 First International Conference of Intelligent Computing and Engineering (ICOICE)*, Hadhramout, Yemen, pp. 1-4, 2019.

[9] L. Sevgi, "Electromagnetic diffraction modeling: High frequency asymptotics vs. numerical techniques," *Applied Computational Electromagnetics Society Journal*, vol. 32, no. 7, pp. 555-561, 2017.

[10] D. Shi, N. Lv, N. Wang, and Y. Gao, "An improved shooting and bouncing ray method for outdoor wave propagation prediction," *Applied Computational Electromagnetics Society Journal*, vol. 32, no. 7, pp. 581-585, 2017.

[11] T. A. Thomas, M. Rybakowski, S. Sun, T. Rappaport, H. Nguyen, I. Kovacs, and I. Rodriguez, "A prediction study of path loss models from 2–73.5 GHz in an urban-macro environment," *Proc. IEEE 83rd VTC Spring*, May 2016.

[12] S. Sun, G. R. MacCartney, and T. S. Rappaport, "Millimeter-wave distance-dependent large-scale propagation measurements and path loss models for outdoor and indoor 5G systems," *Proc. 10th EuCAP*, Apr. 2016.

[13] O. Ozgun, "Modeling of diffraction effects in urban radiowave propagation," *Applied Computational Electromagnetics Society Journal*, vol. 32, no. 7, pp. 593-599, 2017.

[14] D. Shi, N. Lv, and Y. Gao, "A diffraction ray tracing method based on curved surface ray tube for complex environment," *Applied Computational Electromagnetics Society Journal*, vol. 32, no. 7, pp. 608-613, 2017.

[15] L. Azpilicueta, M. Rawat, K. Rawat, F. Ghannouchi, and F. Falcone, "Convergence analysis in deterministic 3D ray launching radio channel estimation in complex environments," *Applied Computational Electromagnetics Society Journal*, vol. 29, no. 4, pp. 256-271, 2014.

[16] M. K. Samimi and T. S. Rappaport, "3-D statistical channel model for millimeter-wave outdoor mobile broadband communications," *2015 IEEE International Conference on Communications (ICC)*, London, pp. 2430-2436, 2015.

[17] F. Fuschini, H. El-Sallabi, V. Degli-Esposti, L. Vuokko, D. Guiducci, and P. Vainikainen, "Analysis of multipath propagation in urban environment through multidimensional measurements and advanced ray tracing simulation," *in IEEE Transactions on Antennas and Propagation*, vol. 56, no. 3, pp. 848-857, 2008.

[18] K. Tateishi, D. Kunta, A. Harada, Y. Kishryama, S. Parkvall, E. Dahlman, and J. Furuskg, "Field experiments on 5G radio access using 15-GHz band in outdoor small cell environment," *2015 IEEE 26th Annual International Symposium on Personal, Indoor, and Mobile Radio Communications (PIMRC)*, Hong Kong, pp. 851-855, 2015.

[19] D. N. Schettino, F. J. S. Moreira, and C. G. Rego, "Efficient ray tracing for radio channel characterization of urban scenarios," *in 12th Biennial IEEE Conference on Electromagnetic Field Computation*, Miami, FL, pp. 267-271, 2006.

[20] W. Tang, H. Cha, M. Wei, B. Tian, and Y. Li, "A study on the propagation characteristics of AIS signals in the evaporation duct environment," *2018 International Applied Computational Electromagnetics Society Symposium - China (ACES)*, Beijing, China, pp. 1-2, 2018.

[21] D. Shi, X. Tang, C. Wang, M. Zhao, and Y. Gao, "A GPU implementation of a shooting and bouncing ray tracing method for radio wave propagation," *Applied Computational Electromagnetics Society Journal*, vol. 32, no. 7, pp. 614-619, 2017.

[22] L. M. Frazier, "Radar surveillance through solid materials," *in Proceedings of the SPIE - The International Society for Optical Engineering*, vol. 2938, Hughes Missile Syst. Co., Rancho Cucamonga, CA, USA, pp. 139-146, 1997.

[23] R. Wilson, "Propagation losses through common building materials 2.4 GHz vs 5 GHz," *University of Southern California*, CA, Tech. Rep. E10589, Aug. 2002.

[24] M. U. Sheikh and J. Lempiainen, "Analysis of outdoor and indoor propagation at 15 GHz and millimeter wave frequencies in microcellular environment," *Advances in Science, Technology and Engineering Systems Journal*, vol. 3, no. 1, pp. 160-167, 2018.

[25] C. Bas, R. Wang, S. Sangodoyin, T. Choi, S. Hur, K. Whang, J. Park, C. Zhang, and A. Molisch, "Outdoor to indoor propagation channel measurements at 28 GHz," *in IEEE Transactions on Wireless Communications*, vol. 18, no. 3, pp. 1477-1489, 2019.

[26] T. Imai, K. Kitao, N. Tran, N. Omaki, Y. Okumura, and K. Nishimori, "Outdoor-to-Indoor path loss modeling for 0.8 to 37 GHz band," *2016 10th European Conference on Antennas and Propagation (EuCAP)*, Davos, pp. 1-4, 2016.